# Quasi-Ballistic Thermal Transport Across MoS₂ Thin Films

Aditya Sood,*,†,‡,◆ Feng Xiong,§ Shunda Chen,‖ Ramez Cheaito,‡ Feifei Lian,†,¶ Mehdi Asheghi,‡ Yi Cui,⊥,# Davide Donadio,‖,∇ Kenneth E. Goodson,‡,⊥ and Eric Pop*,†,⊥,○

†Department of Electrical Engineering, Stanford University, Stanford, California 94305, United States

‡Department of Mechanical Engineering, Stanford University, Stanford, California 94305, United States

§Department of Electrical and Computer Engineering, University of Pittsburgh, Pittsburgh, Pennsylvania 15261, United States

‖Department of Chemistry, University of California, Davis, California 95616, United States

⊥Department of Materials Science and Engineering, Stanford University, Stanford, California 94305, United States

#Stanford Institute for Materials and Energy Sciences, SLAC National Accelerator Laboratory, Menlo Park, California 94025, United States

∇Ikerbasque, Basque Foundation for Science, E-48011 Bilbao, Spain

○Precourt Institute for Energy, Stanford University, Stanford, California 94305, United States

S Supporting Information

**ABSTRACT:** Layered two-dimensional (2D) materials have highly anisotropic thermal properties between the in-plane and cross-plane directions. Conventionally, it is thought that cross-plane thermal conductivities ($\kappa_z$) are low, and therefore *c*-axis phonon mean free paths (MFPs) are small. Here, we measure $\kappa_z$ across MoS₂ films of varying thickness (20−240 nm) and uncover evidence of very long *c*-axis phonon MFPs at room temperature in these layered semiconductors. Experimental data obtained using time-domain thermoreflectance (TDTR) are in good agreement with first-principles density functional theory (DFT). These calculations suggest that ∼50% of the heat is carried by phonons with MFP > 200 nm, exceeding kinetic theory estimates by nearly 2 orders of magnitude. Because of quasi-ballistic effects, the $\kappa_z$ of nanometer-thin films of MoS₂ scales with their thickness and the volumetric thermal resistance asymptotes to a nonzero value, ∼10 m² K GW⁻¹. This contributes as much as 30% to the total thermal resistance of a 20 nm thick film, the rest being limited by thermal interface resistance with the SiO₂ substrate and top-side aluminum transducer. These findings are essential for understanding heat flow across nanometer-thin films of MoS₂ for optoelectronic and thermoelectric applications.

**KEYWORDS:** *Phonon, mean free path, MoS₂, cross-plane, thermal conductivity, time-domain thermoreflectance*
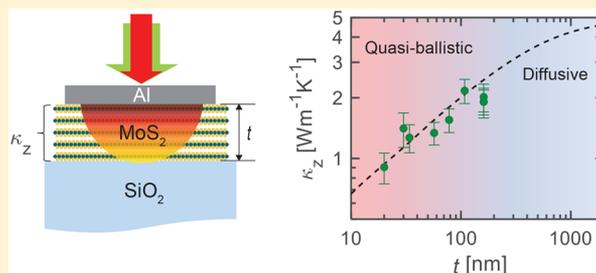
Two-dimensional (2D) van der Waals (vdW) layered solids have highly unusual thermal transport properties due to their unique crystal structure. While atoms within a layer are bonded covalently, adjacent layers are coupled via weak vdW interactions. This leads to a strong anisotropy in thermal conductivity, with the in-plane (along the layers) conductivity $\kappa_r$ being significantly larger than the cross-plane (across the layers, or along the *c*-axis) conductivity $\kappa_z$. For example, in bulk graphite, h-BN, and MoS₂, anisotropy ratios ($\kappa_r/\kappa_z$) as high as ∼300, 200, and 50, respectively, have been reported at room temperature.[1−3] Owing to their high $\kappa_r$, in-plane thermal transport in vdW layered materials has received significant attention, motivated in part by potential applications in heat spreading.[4,5]

In contrast, fundamental aspects of cross-plane thermal transport remain relatively underexplored, despite its relevance to nanoelectronics and energy harvesting applications. For example, self-heating plays a key role in limiting the performance of field effect transistors (FETs) made of 2D

materials.[6,7] While some studies have characterized heat flow at single vdW interfaces,[8−12] very little is known about the physics of "intrinsic" cross-plane thermal transport across multiple vdW layers in layered thin films. Achieving a better understanding of this is critical to realizing the potential of 2D electronics, as previous work on multilayer MoS₂ transistors has shown enhancements in device mobility with increasing channel thickness (up to approximately tens of nanometers).[13,14] In such devices, charge screening and large interlayer electrical resistance can lead to the localization of current within the top few layers,[13] such that the dissipated heat must flow across multiple vdW interfaces before entering the substrate. It is therefore essential to understand the thickness dependence and fundamental limits of cross-plane thermal
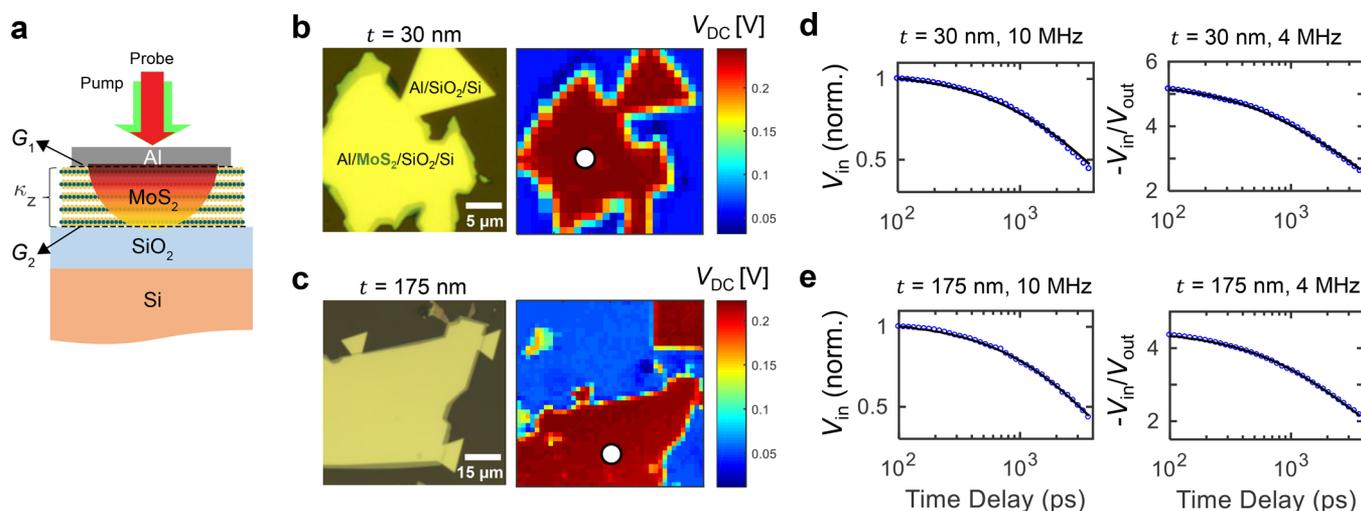
**Figure 1.** (a) Cross-sectional schematic of samples under study, showing the three unknown parameters: $G_1$ (TBC between Al and MoS$_2$), $G_2$ (TBC between MoS$_2$ and SiO$_2$), and $\kappa_z$ (cross-plane thermal conductivity of MoS$_2$). The pump (green, 532 nm) and probe (red, 1064 nm) lasers used for TDTR are shown schematically. (b,c) Top view optical micrographs and probe reflectivity maps (taken at a fixed delay time of 0 ps) for 30 and 175 nm thick MoS$_2$ samples, respectively. Probe reflectivity maps are used to locate a uniform region away from the sample edges, where TDTR measurements are taken (white circles). (d,e) TDTR data (symbols) and best fits (lines): normalized in-phase signal $V_{in}$ at $f_{mod} = 10$ MHz and $-V_{in}/V_{out}$ ratio at $f_{mod} = 4$ MHz for 30 and 175 nm thick films, respectively.

transport in vdW layered solids, particularly in materials like MoS$_2$.

A key quantity that determines thermal transport in the cross-plane direction of a material is the range of phonon mean free paths (MFPs) that carry heat. A simple estimate of the so-called gray MFP ($\Lambda_z$) can be made using the kinetic theory, $\kappa_z \sim (1/3)Cv_z\Lambda_z$; for MoS$_2$, using a heat capacity[15] $C \sim 2$ MJ m$^{-3}$ K$^{-1}$, the average sound velocity of cross-plane acoustic modes[16] $v_z \sim 2400$ ms$^{-1}$, and the cross-plane bulk conductivity[3,17] $\kappa_z \sim 2-5$ W m$^{-1}$ K$^{-1}$, gives a MFP of around 1.5−4 nm, which corresponds to a thickness of 2−6 layers. A similar calculation for graphite gives a gray MFP estimate of around 3 nm, corresponding to 9 layers. This would imply that size effects (i.e., thickness dependence of $\kappa_z$) should be negligible for films thicker than ∼10 nm, i.e. that the cross-plane thermal conductivity should be constant in this thickness regime. However, recent molecular dynamics (MD) simulations[18] and experimental measurements of $\kappa_z$ in graphite[19,20] have suggested surprisingly long $c$-axis MFPs, on the order of approximately hundreds of nanometers.

These studies motivate the following key questions: (1) Are long $c$-axis phonon MFPs a general feature of other vdW-layered systems, like the transition metal dichalcogenides (TMDs) such as MoS$_2$? (2) Can experimental observations of long cross-plane phonon MFPs in vdW materials be explained by first-principles calculations? Density functional theory (DFT) has recently proven to be very effective in understanding fundamental aspects of thermal transport in covalently bonded systems like Si,[21] but similar studies are lacking for vdW-layered solids, especially quantitative comparisons with cross-plane thermal measurements. (3) What is the impact of cross-plane ballistic transport and related size effects on the thermal resistance of thin-film TMD devices? For monolayers, it is understood that interfaces dominate cross-plane transport.[8−11] However, the transition from interface-dominated to bulk-like transport across multilayer TMDs remains unclear to date.

In response, here we probe the spectrum of heat-carrying $c$-axis phonon MFPs in MoS$_2$, a vdW layered semiconductor. Through time-domain thermoreflectance (TDTR)[22] measurements of the thickness-dependent cross-plane thermal conductivity in single-crystalline films, we show that the $c$-axis phonon MFPs are at least ∼10s of nm long, significantly larger than kinetic theory estimates. Using first-principles DFT calculations we uncover that nearly 80% of the heat at room temperature is carried by phonons with MFPs in the range 10 to 500 nm. Furthermore, we show that by suitably defining a characteristic thermal length scale, our thickness-dependent $\kappa_z$ data (with film thickness $t$ ranging from 20 to 240 nm) are consistent with TDTR data on bulk MoS$_2$ crystals reported previously[3,17,23] (with thermal penetration depth $d_p$ ranging from 200 nm to 1 $\mu$m). Taken together, we find good agreement between the combined data set and DFT predictions over a broad spectrum of thermal length scales, from 20 nm to 1 $\mu$m. Finally, using our measured values of the metal/MoS$_2$ and MoS$_2$/substrate interface resistances, we estimate the impact of cross-plane quasi-ballistic phonon transport on the total thermal resistance of multilayer MoS$_2$ devices. These calculations reveal that contrary to what is typically assumed, the total thermal resistance of few nanometer thick films is not entirely interface-dominated; the lower limit is set by the ballistic resistance across the thickness of MoS$_2$, which is estimated to be ∼10 m$^2$ K GW$^{-1}$.

**Experimental Procedure.** Single crystalline MoS$_2$ films were exfoliated onto SiO$_2$ (90 nm) on p-doped Si substrates using micromechanical exfoliation. Exfoliation yielded several MoS$_2$ films of different thicknesses on a single ∼1 cm$^2$ chip. Suitable films were identified using optical microscopy, and their thicknesses measured using atomic force microscopy (AFM). An ∼80 nm thick Al transducer was patterned and deposited onto the samples using electron-beam (e-beam) lithography and e-beam evaporation, respectively, for TDTR measurements (see sample schematic in Figure 1a and Methods). We also patterned Al onto bare regions of the SiO$_2$/Si substrate adjacent to the MoS$_2$ during the same
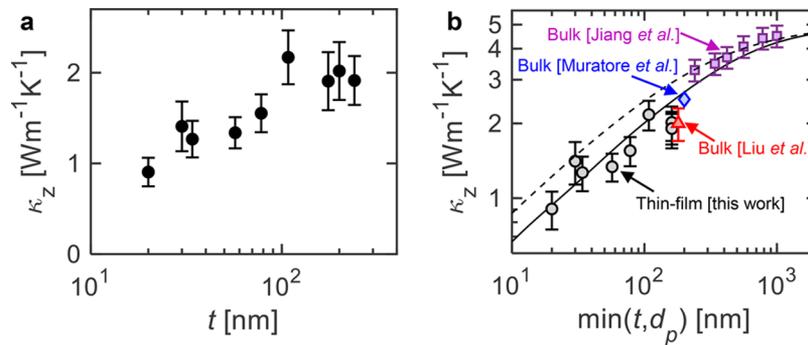
**Figure 2.** (a) Measured intrinsic cross-plane thermal conductivity $\kappa_z$ versus film thickness $t$. (b) Experimental data plotted as a function of the characteristic thermal length scale, which is the smaller of the thickness ($t$) and thermal penetration depth ($d_p$). For our measurements, $d_p \approx 160$ nm in the three thickest films at $f_{mod} = 4$ MHz. Also shown are prior TDTR measurements of bulk $MoS_2$ by Liu et al.[3] (red triangle), Muratore et al.[23] (blue diamond), and Jiang et al.[17] (magenta squares). Solid and dashed lines are predictions of first-principles DFT calculations with suppression functions based on the BTE[20] (eq 2) and Matthiessen's rule (eq 3), respectively.

evaporation step. This allowed us to perform reference measurements of the $SiO_2$ next to each set of samples, and helped calibrate the accuracy and consistency of our setup.

Thermal transport measurements were made using TDTR, which is a well-established optical pump-probe technique capable of measuring thermal transport in thin films and across interfaces. Details of this technique and our setup have been described previously.[22] In these experiments, the pump beam was modulated at frequencies $f_{mod} = 4$ and 10 MHz. We used a high-magnification 50× objective lens that produced a focused root-mean-square (rms) spot size ($1/e^2$ diameter) of $w_0 \approx 3$ $\mu$m. An integrated dark-field microscope helped locate the samples under the laser spot.[24] Because some of the samples have lateral dimensions as small as 15 $\mu$m (especially for the thinnest films), it is important to position the laser spot well inside the edges of the flake. To do this, a precision two-axis translation stage was used to map out the TDTR signal and probe beam reflectivity over the area of the sample at a fixed delay time (see Figure 1b,c). A spot was chosen at the center of the sample within a region where the TDTR lock-in voltages and probe reflectivity were uniform, and TDTR scans were taken at that location with pump-probe delay times of 100 ps to 3.7 ns. The analysis scheme discussed below was used to simultaneously fit the normalized in-phase signal $V_{in}$, and the ratio ($= -V_{in}/V_{out}$) to a three-dimensional (3D) heat diffusion model that considers anisotropic transport.[1]

The sample stack consists of $Al/MoS_2/SiO_2/Si$ (see Figure 1a). The thicknesses of Al and $MoS_2$ were measured using AFM, while the $SiO_2$ thickness was characterized using ellipsometry to be $90 \pm 1$ nm. All measurements were performed at room temperature. The thermal conductivity of Al was estimated using in-plane electrical conductivity measurements on a patterned 4-probe device and the Wiedemann–Franz law, $\kappa_{Al} \approx 170$ W m$^{-1}$ K$^{-1}$. The thermal conductivity of the p-type Si substrate, and volumetric specific heat of Al, $SiO_2$, $MoS_2$ and Si were taken from literature.[15,25−28] To reduce the uncertainties associated with slight variations in the laser spot size between measurements on different samples, reference data were taken on the $Al/SiO_2/Si$ regions next to each flake. Adjustments were made in the spot size (<5% variation across samples) to keep the fitted $SiO_2$ thermal conductivity fixed at 1.4 W m$^{-1}$ K$^{-1}$. No $f_{mod}$ dependence was observed in the thermal conductivity of $SiO_2$ and thermal boundary conductance (TBC) of the $Al/SiO_2$

interface ($\approx 130$ MW m$^{-2}$ K$^{-1}$) for modulation frequencies between 4 and 10 MHz.

In the $MoS_2$ sample stack, there are four unknown parameters for each sample thickness $t$. They are the intrinsic cross-plane and in-plane thermal conductivities of the $MoS_2$ layer, $\kappa_z$ and $\kappa_r$, and the TBCs at the $Al/MoS_2$ and $MoS_2/SiO_2$ interfaces, $G_1$ and $G_2$, respectively. The in-plane thermal conductivity is held fixed at $\kappa_r = 90$ W m$^{-1}$ K$^{-1}$, based on prior measurements of bulk $MoS_2$ crystals by Liu et al.[3] Here, the authors had measured a spot-size dependent $\kappa_r$, likely due to the partial exclusion of ballistic phonons with in-plane MFPs larger than the spot diameter. Our estimate for $\kappa_r$ is obtained by linearly interpolating their data to an rms spot diameter of 3 $\mu$m. To simplify our analysis we assume that $\kappa_r$ is independent of $t$, at least within the range of thicknesses (20 nm < $t$ < 240 nm) measured here. This is consistent with previous arguments by Minnich[29] and Gu et al.,[30] an assump-assumption further discussed below.

This assumption leaves three unknown parameters for each sample: $\kappa_z$, $G_1$, and $G_2$. To extract a unique value for $\kappa_z$, we use a combination of $V_{in}$ and ratio ($= -V_{in}/V_{out}$) signals, at two different modulation frequencies, 4 and 10 MHz. This tandem fitting approach is similar to that used by Meyer et al.[31] and is supported by our sensitivity analysis (see Supporting Information Section 1). For films with $t$ < 150 nm, we first estimate $G_1$ by fixing $\kappa_z$ and $G_2$ and fitting the in-phase signal $V_{in}$ (normalized at +100 ps) at the higher $f_{mod}$ of 10 MHz. Next, fixing $G_1$ at this value, the voltage ratio data at the lower $f_{mod}$ of 4 MHz are fit for $\kappa_z$ and $G_2$. This process is repeated until the values of $\kappa_z$, $G_1$, and $G_2$ each change by less than 1% between successive iterations. We verify that the final fit results are not sensitive to the choice of initial values. For films with $t$ > 150 nm, measurement sensitivity to the bottom interface TBC, $G_2$, is relatively low. For these, we follow the same procedure as above, except that $G_2$ is held fixed at $21 \pm 5$ MW m$^{-2}$ K$^{-1}$ based on the thin film results, further discussed below. Our methodology is generally similar to that used by Zhang et al.[20] and Jang et al.[32] for thickness-dependent $\kappa_z$ measurements of graphite and black phosphorus, respectively. Error bars are calculated by propagating uncertainties in the assumed thermophysical parameters, mainly the Al thickness ($\pm 1$ nm) and rms laser spot size ($\pm 2$%), and for the thick films also $G_2$ ($\pm 5$ MW m$^{-2}$ K$^{-1}$).

We note that a recent experimental study[33] reported thickness-dependent in-plane thermal conductivity of $MoS_2$
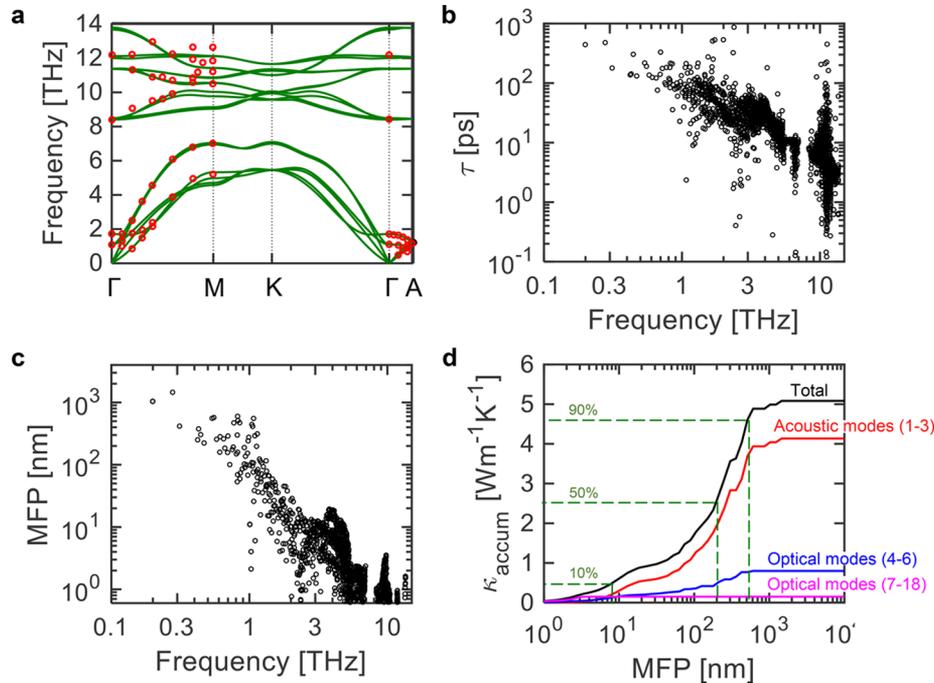
**Figure 3.** First-principles DFT calculations of MoS$_2$. (a) Phonon dispersion relations along high-symmetry directions in the Brillouin zone. Also shown with red circles are experimental data from neutron scattering on bulk MoS$_2$ crystals.[43] (b) Calculated phonon relaxation times, and (c) mean free paths (MFPs), plotted versus phonon frequency. (d) MFP accumulation function obtained from DFT calculations. The black curve is the total cross-plane thermal conductivity; the red, blue, and magenta curves are the contributions of the acoustic modes (branches 1−3, from low to high frequency on the dispersion relation), the three lowest-lying optical modes (branches 4−6), and the remaining higher-frequency optical modes (branches 7−18). Green dashed lines indicate MFPs corresponding to 10, 50, and 90% of the accumulated total thermal conductivity.

films in the range 2.4 to 37.8 nm. To check whether this thickness-dependence might affect our extraction of $\kappa_z$, we also analyzed our data using $\kappa_r$ estimated from these results. For the 20 and 34 nm thick films, the resulting change in $\kappa_z$ is only ~2% and ~12%, respectively. These uncertainties are within the experimental error bars; this further confirms that our assumption of constant $\kappa_r$ for all films does not affect the extracted trend of $\kappa_z$ versus $t$.

**Results and Discussion.** Representative TDTR data and model best fits for 30 and 175 nm thick samples are shown in Figure 1d,e, respectively. Figure S2 shows the extracted top and bottom interface TBCs, $G_1$ and $G_2$ versus $t$. The MoS$_2$/SiO$_2$ TBCs fall within a narrow range of 16 to 26 MW m$^{-2}$ K$^{-1}$, in reasonable agreement with Raman thermometry measurements of monolayer MoS$_2$ on SiO$_2$ (14 ± 4 MW m$^{-2}$ K$^{-1}$) by Yalon et al.[8,9] The Al/MoS$_2$ TBCs are in general higher than MoS$_2$/SiO$_2$ TBCs and also show a larger spread from 30 to 80 MW m$^{-2}$ K$^{-1}$ with no systematic trend as a function of $t$. This larger variability in $G_1$ could be a result of varying degrees of surface cleanliness after the e-beam patterning process that is used to define the Al transducer.

Figure 2a plots the extracted cross-plane thermal conductivity $\kappa_z$ as a function of layer thickness $t$; $\kappa_z$ for the thickest film ($t$ = 240 nm) is 2.0 ± 0.3 W m$^{-1}$ K$^{-1}$. This decreases with decreasing film thickness down to 0.9 ± 0.2 W m$^{-1}$ K$^{-1}$ for $t$ = 20 nm, more than a two-fold reduction. Such a dependence of $\kappa_z$ on $t$ is indicative of quasi-ballistic $c$-axis phonon transport and suggests that the dominant heat-carrying vibrational modes have MFPs of at least tens of nanometers. We note that $\kappa_z$ appears to saturate for the three thickest films. As discussed further below, we posit that this occurs due to the finite thermal penetration depth of the TDTR measurement.

Our measured $\kappa_z$ values for the thickest films are close to two prior measurements of bulk MoS$_2$ by Liu et al.[3] and Muratore et al.[23] who obtained $\kappa_z$ of ~2 W m$^{-1}$ K$^{-1}$, and ~2.5 W m$^{-1}$ K$^{-1}$, respectively, using a TDTR modulation frequency of 9.8 MHz.[34] However, these two results are significantly lower than recent measurements by Jiang et al.,[17] who obtained a bulk $\kappa_z$ ~4.8 W m$^{-1}$ K$^{-1}$. In addition, our first-principles DFT calculations (described later) obtain a bulk $\kappa_z$ ~5 W m$^{-1}$ K$^{-1}$, which is in good agreement with the experimental result of Jiang et al.[17] and a recent DFT calculation by Lindroth et al.[16] that predicted $\kappa_z$ ~5.1 W m$^{-1}$ K$^{-1}$.

To understand possible reasons behind the apparent discrepancy among the different bulk $\kappa_z$ measurements and first-principles calculations, we consider the characteristic thermal length scale (i.e., length scale over which the temperature gradient occurs) in the experiments. For TDTR measurements made at a frequency $f_{mod}$, this is determined by the thermal penetration depth[35] $d_p$, which is approximately $\sqrt{\kappa_z/\pi C f_{mod}}$. To calculate $d_p$ accurately, we solve the full 3D heat diffusion equation in the two-layer Al/MoS$_2$ stack (see Supporting Information Section 3).

For the case of Liu et al.[3] and Muratore et al.,[23] this gives $d_p$ ~ 180 nm (for $\kappa_z$ ~2 W m$^{-1}$ K$^{-1}$), and $d_p$ ~ 200 nm (for $\kappa_z$ ~2.5 W m$^{-1}$ K$^{-1}$), respectively, at $f_{mod}$ = 9.8 MHz. Jiang et al.[17] performed TDTR measurements of $f_{mod}$-dependent $\kappa_z$ in bulk MoS$_2$, and observed a reduction in the apparent $\kappa_z$ from 4.5 to 3.3 W m$^{-1}$ K$^{-1}$ while increasing $f_{mod}$ from 1 to 10 MHz. These results were interpreted based on a two-channel model that considers nonequilibrium effects between low and high-frequency phonons that have different thermal conductivities and heat capacities. The interpretation of $f_{mod}$-dependent $\kappa_z$ in modulated opto-thermal measurements has been the topic of
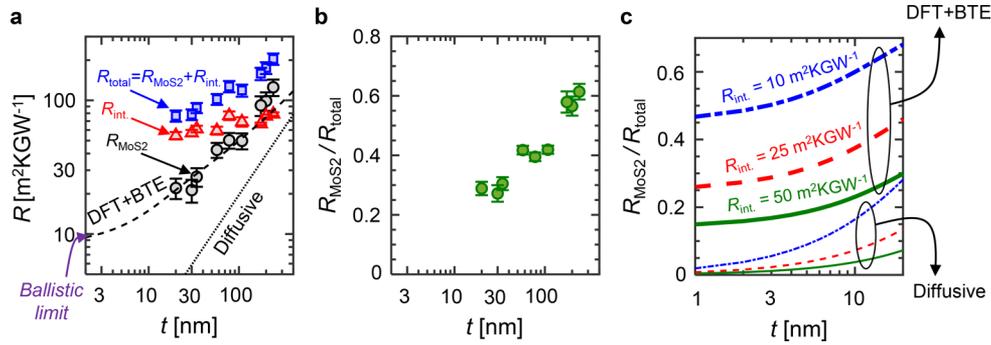
**Figure 4.** (a) Cross-plane thermal resistance of the MoS$_2$ film $R_{MoS2} = t/\kappa_z$ (black circles), combined thermal resistance of Al/MoS$_2$ and MoS$_2$/SiO$_2$ interfaces $R_{int.} = 1/G_1 + 1/G_2$ (red triangles), and total thermal resistance $R_{total} = R_{MoS2} + R_{int.}$ (blue squares), plotted versus film thickness $t$. The dashed line is the calculated quasi-ballistic $R_{MoS2}$ based on first-principles MFPs (Figures 3c,d) and BTE suppression function (eq 2), while the dotted line is the corresponding diffusive calculation assuming a constant $\kappa_z = 5.1$ W m$^{-1}$ K$^{-1}$. The y-intercept of the dashed line denotes the intrinsic cross-plane resistance in the ballistic limit $\approx 10$ m$^2$ K GW$^{-1}$. (b) Fractional thermal resistance of the MoS$_2$ film compared to the total resistance (= $R_{MoS2}/R_{total}$) plotted versus $t$. (c) Calculated fractional resistance contributed by the MoS$_2$ film for sub-20 nm thicknesses. The quasi-ballistic (heavy lines) and diffusive case (light lines) are calculated in a manner similar to (a). Three cases are shown, corresponding to $R_{int.} = 10$, 25, and 50 m$^2$ K GW$^{-1}$ in the blue dash-dotted, red dashed, and green solid lines, respectively.

much recent discussion.[17,25,35−40] While the treatment of near-interfacial phonon nonequilibrium deserves further attention, a first order approximation is that the contributions to heat transport of long MFP phonons with $\Lambda_z > d_p$ are suppressed at high $f_{mod}$, thereby lowering the measured apparent $\kappa_z$. This simplification is reasonable for low thermal conductivity solids with relatively broad MFP spectra, as was discussed recently in the context of black phosphorus by Sun et al.,[41] and applied quantitatively to low thermal conductivity semiconductor alloys by Koh et al.[35]

In this simplified picture, we replot our thin-film $\kappa_z$ data, along with the bulk data of Liu et al.,[3] Muratore et al.,[23] and Jiang et al.,[17] against the thermal characteristic length scale (the smaller of $t$ and $d_p$) as shown in Figure 2b. For our thin-film samples, $d_p$ is calculated using a numerical solution of the 3D heat diffusion equation in the four-layer stack (Al/MoS$_2$/SiO$_2$/Si). For most of our films, $d_p$ is larger than $t$. However, for the three thickest films $d_p \approx 160$ nm, which is smaller than $t$ (= 175, 200, 240 nm). Details of these calculations are provided in the Supporting Information Section 3. Following this procedure, a combined data set is obtained, where $\kappa_z$ increases from ~0.9 to ~5 W m$^{-1}$ K$^{-1}$ for thermal length scales ranging from 20 nm to 1 $\mu$m. This analysis suggests that one possible reason for the discrepancy between different bulk measurements[3,17,23] could be the dependence of $\kappa_z$ on modulation frequency and the finite thermal penetration depth. However, given that the source of MoS$_2$ crystals is typically geological, one cannot entirely rule out differences in sample quality between the various studies as contributing to the observed $\kappa_z$ variations.

Also shown in Figure 2b is a prediction of $\kappa_z$ from first-principles calculations (described below), where the effect of finite thickness is incorporated with a suppression function calculated by the Boltzmann transport equation[20] (BTE) and Matthiessen's rule. These predictions show reasonably good agreement with the combined data set over the full range of characteristic thermal length scales from 20 nm to 1 $\mu$m. The data are thus consistent with theoretical predictions of very long c-axis phonon MFPs, and a broad spectral distribution of vibrational modes.

**First-Principles DFT Calculations.** To gain insight into fundamental aspects of phonon transport processes in MoS$_2$, we perform first-principles DFT calculations in the local density approximation of the exchange and correlation functional. We compute the frequency- and MFP-resolved $\kappa_z$ of MoS$_2$ by solving the phonon BTE with an iterative self-consistent algorithm.[42] Further details are provided in Methods and Chen et al.[42]

Calculated phonon dispersion curves for 2H-MoS$_2$ are shown in Figure 3a, which are in good agreement with experimental data.[43] Figure 3b,c plots the calculated phonon relaxation times and MFPs as a function of phonon frequency. The MFP accumulation function $\kappa_{accum}$ is calculated as a cumulative integral of the contributions to the total thermal conductivity of phonons with MFPs smaller than a certain value and is plotted in Figure 3d. From these calculations, we infer that more than 50% of the heat at room temperature is carried by phonons with MFPs exceeding 200 nm and nearly 80% is carried by MFPs in the range 10 to 500 nm. In comparison, in silicon,[21] 80% of the heat at room temperature is carried by phonons with MFPs between 40 nm and 10 $\mu$m.

On the basis of the MFP accumulation function, we calculate the cross-plane thermal conductivity of a film of thickness $t$ as follows

$$\kappa_z(t) = \int_0^\infty S(Kn_\omega)\kappa_{partial}(\Lambda_{z,\omega})d\Lambda_{z,\omega}$$

$$= \int_0^\infty \frac{1}{t}N(Kn_\omega)\kappa_{accum}(\Lambda_{z,\omega})d\Lambda_{z,\omega} \quad (1)$$

where $\kappa_{partial}(\Lambda_{z,\omega})$ is the MFP partial contribution function, $Kn_\omega = \Lambda_{z,\omega}/t$ is the Knudsen number, $S(Kn_\omega)$ is the heat flux suppression function, $\kappa_{accum}(\Lambda_{z,\omega}) = \int_0^{\Lambda_{z,\omega}} \kappa_{partial}(\Lambda_{z,\omega})d\Lambda_{z,\omega}$ is the MFP accumulation function, and $N(Kn_\omega) = -dS(Kn_\omega)/dKn_\omega$. Two cases are considered for the suppression function $S(Kn_\omega)$: one is based on a solution to the BTE for cross-plane heat flow in an anisotropic film inspired by the Fuchs–Sondheimer model[20] (eq 2), and the other is based on Matthiessen's rule (eq 3)

$$S_{BTE}(Kn_\omega) = 1 - Kn_\omega\left(1 - \exp\left(-\frac{1}{Kn_\omega}\right)\right) \quad (2)$$

$$S_{\text{Matth.}}(Kn_\omega) = \frac{1}{1 + Kn_\omega} \qquad (3)$$

These are plotted as solid and dashed lines, respectively, in Figure 2b and show good agreement with the experimental $\kappa_z$ data over a large range of characteristic thermal length scales. These results have important implications for the design of thermoelectric devices based on vdW materials, as they suggest that cross-plane heat conduction can be suppressed significantly by the incorporation of defects along the $c$-axis,[42,44,45] such as intercalants and rotationally mismatched layers. The large phonon MFPs predicted and experimentally confirmed here offer a route to high-efficiency thermoelectrics based on nanostructuring of layered 2D materials along the $c$-axis.

**Implications for 2D Device Thermal Characteristics.** To understand the impact of cross-plane ballistic phonon transport on thermal characteristics of thin-film $MoS_2$ electronic and optoelectronic devices, in Figure 4a we plot the volumetric cross-plane thermal resistance $R_{MoS2} = t/\kappa_z$, the combined interface resistance ($Al/MoS_2$ and $MoS_2/SiO_2$) $R_{\text{int.}}$ = $1/G_1 + 1/G_2$, and the total thermal resistance $R_{\text{total}} = R_{MoS2} + R_{\text{int.}}$, as a function of thickness $t$. This simplification assumes that the total resistance can be decomposed into the separate interfacial and volumetric contributions even though a large fraction of phonons undergoes quasi-ballistic transport across the thickness of the $MoS_2$ film. This assumption, which is also inherent to our data analysis methodology, is consistent with the approach commonly followed in literature when dealing with subcontinuum heat conduction across thin films.[20]

We find that $R_{MoS2}$ decreases with decreasing thickness but does not go to zero in the limit of zero $t$. This is a direct consequence of quasi-ballistic phonon transport and the diffusive scattering of long MFP phonons at the $Al/MoS_2$ and $MoS_2/SiO_2$ interfaces. In Figure 4a, we also plot the calculated $MoS_2$ volumetric resistance as a function of thickness, based on DFT predictions of the phonon MFPs and the BTE suppression function (eq 2). Because of ballistic transport across the film thickness, $R_{MoS2}$ saturates at a finite value of ~10 m$^2$ K GW$^{-1}$ in the limit of 2−3 monolayers. In the absence of quasi-ballistic effects, i.e., in the diffusive regime, $R_{MoS2}$ would have been significantly lower and become vanishingly small in the monolayer limit.

An important consequence of quasi-ballistic effects is that the total thermal resistance is not dominated entirely by the interfaces, even for thin films. In Figure 4b we plot the fractional contribution of the volumetric $MoS_2$ resistance to the total device resistance (= $R_{MoS2}/R_{\text{total}}$) versus $t$. In our experiments, for the thinnest film ($t$ = 20 nm), $R_{MoS2} \approx 22$ m$^2$ K GW$^{-1}$ and $R_{\text{total}} \approx 76$ m$^2$ K GW$^{-1}$, i.e., nearly 30% of the total thermal resistance is due to the volumetric component. In the diffusive limit with constant $\kappa_z = 5.1$ W m$^{-1}$ K$^{-1}$, this value is only 7% (i.e., the interfaces contribute 93%) for a 20 nm thick film. From a metrology perspective, an important consequence of this effect is our ability to experimentally measure the intrinsic component $\kappa_z$ separately from the interface resistances, down to films as thin as 20 nm. If thermal transport were to remain diffusive, the volumetric resistance component would have been too small compared to the interface resistances, and we would not have been able to extract it uniquely using TDTR.

To estimate the contribution of quasi-ballistic transport to heat flow across thin devices ($t < 20$ nm), we plot the fractional $MoS_2$ volumetric component for different interface resistance values ($R_{\text{int.}}$= 10, 25, 50 m$^2$ K GW$^{-1}$), as shown in Figure 4c. As before, size effects are considered by calculating the thickness-dependent $\kappa_z$ using the BTE suppression function described in eq 2 above. In the extreme scaling limit of 1−2 nm thick films (2−3 monolayers), we estimate this fractional contribution to be as large as ~15%, ~25%, and ~50% for $R_{\text{int.}}$= 50, 25, and 10 m$^2$ K GW$^{-1}$, respectively. This suggests that even if interface quality (and TBCs) of the metal/$MoS_2$ and $MoS_2$/substrate interfaces were to be improved substantially ($R_{\text{int.}} \rightarrow 0$), cross-plane heat transport would likely still be limited by the ballistic resistance (= $\lim_{t \to 0} t/\kappa_z$) of the $MoS_2$ film, which is ~10 m$^2$ K GW$^{-1}$. Note that this analysis assumes a 3D phonon dispersion for thin films, which may face its limits when the thickness becomes comparable to the phonon wavelengths (see Supporting Information Section 4). Nevertheless, this raises interesting questions about the nature of heat conduction across few-layer thick vdW layered materials, where it is often assumed that interfaces dominate the total cross-plane thermal resistance.[46] Given that the existence of long MFP $c$-axis thermal phonons has been experimentally demonstrated in graphite[19,20] and predicted theoretically in other TMDs such as $WS_2$ and $WSe_2$,[16] the above argument may be applicable to a large class of ultrathin vdW layered devices (see Supporting Information Section 5).

In conclusion, we reported thickness-dependent cross-plane thermal conductivity measurements of crystalline films of layered $MoS_2$. The cross-plane thermal conductivity shows a strong dependence on thickness in the range of 20−240 nm, revealing quantitative information about the distribution of phonon MFPs along the $c$-axis. Combining our results with previous measurements[3,17,23] of $\kappa_z$ in bulk $MoS_2$ (made at different modulation frequencies) allowed us to map a large portion of the $c$-axis MFP spectrum from ~20 nm to ~1 $\mu$m. DFT calculations (with no fitting parameters) were able to obtain the thickness-dependent thermal conductivity over a large range of MFPs, illustrating the predictive power of first-principles phonon calculations for vdW layered materials.

Importantly, our results show for the first time that diffuse scattering of long MFP phonons imposes a lower limit on the cross-plane thermal resistance of vdW layered thin films. This can have significant implications for the thermal management of multilayer 2D electronics[13,47] and optoelectronics (e.g., photovoltaics) where thermal transport across the device thickness imposes the primary bottleneck for heat dissipation. Finally, the quantitative knowledge of thermal phonon MFPs obtained here will enable the design of new applications that require engineering of the phonon spectrum. For example, the substantial contribution of long MFP phonons to $\kappa_z$ suggests that the introduction of disorder and defects along the $c$-axis can drastically suppress cross-plane thermal transport[45] without significantly affecting electronic transport. This could have exciting implications for cross-plane thermoelectrics made of layered 2D materials,[48] potentially enabling next-generation energy harvesting and electronics cooling technologies.

**Methods.** *Sample Preparation.* Flakes of $MoS_2$ were mechanically exfoliated from bulk crystals (SPI Supplies) onto 90 nm $SiO_2$ on p-type Si substrates (0.001 to 0.005 $\Omega$.cm) using a thermal release tape (Nitto-Denko Revalpha). Samples were cleaned with an acetone/2-propanol soak and subsequently annealed in Ar/H$_2$ at 400 °C for 40 min. This was followed by spin coating a double layer of electron-beam (e-beam) resist PMMA 495 K A2/950 K A4 (Microchem).

The metal transducer (nominally 80 nm Al) was patterned by e-beam lithography (Raith 150, 10 kV) and deposited through e-beam evaporation. Lift-off was performed in acetone at 50 °C.

*Ab Initio Calculations.* First-principles phonon calculations of 2H-MoS$_2$ were carried out in the local density approximation (LDA) of the exchange and correlation functional using the Quantum-Espresso package.[49,50] Norm-conserving pseudopotentials were used to approximate core electrons.[51] Kohn−Sham wave functions were expanded on a plane wave basis set (cutoff = 100 Ry). Integration of the electronic properties over the first Brillouin zone was performed using 10 × 10 × 4 Monkhorst−Pack meshes of k-points.[52] Structural and cell relaxations were performed by a Broyden−Fletcher−Goldfarb−Shanno quasi-Newton algorithm with a strict convergence criterion of $10^{-8}$ Rydberg/Bohr for maximum residual force component.

Phonon dispersion relations were computed by density functional perturbation theory (DFPT)[53] with 10 × 10 × 4 q-point mesh (see Figure 3a). The computed dispersion curves agree well with neutron diffraction data for bulk MoS$_2$.[43] For the calculation of lattice thermal conductivity, anharmonic third order interatomic force constants (IFCs) are also necessary besides the harmonic second order IFCs. Third order anharmonic force constants were computed by finite differences for a supercell,[54] which is a 5 × 5 × 1 replica of the unit cell and contains 150 atoms, with an interaction cutoff of 7 Å, including interactions up to the tenth shell of neighbors. Translational invariance of the anharmonic force constants was enforced using the Lagrangian approach.[54] With the second and third order IFCs, the thermal conductivity of MoS$_2$ was computed by solving the phonon BTE with an iterative self-consistent algorithm, using the ShengBTE code,[54] considering phonon−phonon and isotopic scattering. Convergence was checked with q-point grids up to 45 × 45 × 11. Further details are provided in Chen et al.[42]

## ASSOCIATED CONTENT

**ⓢ Supporting Information**

The Supporting Information is available free of charge on the ACS Publications website at DOI: 10.1021/acs.nano-lett.8b05174.

TDTR sensitivity analysis. Thermal boundary conductance (TBC) measurements of Al/MoS$_2$ and MoS$_2$/SiO$_2$ interfaces. Calculations of thermal penetration depth. Phonon wavelength contributions to cross-plane thermal conductivity. Literature survey of cross-plane thermal resistance of few-layer graphene and thin-film graphite (PDF)

## AUTHOR INFORMATION

**Corresponding Authors**

*E-mail: aditsood@alumni.stanford.edu.

*E-mail: epop@stanford.edu.

**ORCID ⓘ**

Aditya Sood: 0000-0002-4319-666X

Shunda Chen: 0000-0002-5506-7507

Yi Cui: 0000-0002-6103-6352

Davide Donadio: 0000-0002-2150-4182

Eric Pop: 0000-0003-0436-8534

**Present Addresses**

◆(A.S.) Stanford Institute for Materials and Energy Sciences, SLAC National Accelerator Laboratory, Menlo Park, CA 94025, USA.

¶(F.L.) NG Next Basic Research Laboratory, Northrop Grumman Corporation, Redondo Beach, CA 90278, USA.

**Author Contributions**

A.S. and F.X. contributed equally. A.S., F.X., and E.P. conceived the project. A.S. designed and performed the TDTR measurements, analyzed experimental data, developed the theoretical model based on DFT calculations, and wrote the manuscript with input from E.P.; F.X. fabricated the samples; S.C. performed the DFT calculations; R.C. and F.L. provided inputs on data analysis; M.A., Y.C., D.D., K.E.G., and E.P. supervised the project.

**Notes**

The authors declare no competing financial interest.

## ACKNOWLEDGMENTS

## REFERENCES

(1) Schmidt, A. J.; Chen, X.; Chen, G. Pulse Accumulation, Radial Heat Conduction, and Anisotropic Thermal Conductivity in Pump-Probe Transient Thermoreflectance. *Rev. Sci. Instrum.* **2008**, *79*, 114902.

(2) Sichel, E. K.; Miller, R. E.; Abrahams, M. S.; Buiocchi, C. J. Heat Capacity and Thermal Conductivity of Hexagonal Pyrolytic Boron Nitride. *Phys. Rev. B* **1976**, *13* (10), 4607−4611.

(3) Liu, J.; Choi, G. M.; Cahill, D. G. Measurement of the Anisotropic Thermal Conductivity of Molybdenum Disulfide by the Time-Resolved Magneto-Optic Kerr Effect. *J. Appl. Phys.* **2014**, *116*, 233107.

(4) Song, H.; Liu, J.; Liu, B.; Wu, J.; Cheng, H. M.; Kang, F. Two-Dimensional Materials for Thermal Management Applications. *Joule* **2018**, *2* (3), 442−463.

(5) Sood, A.; Pop, E.; Asheghi, M.; Goodson, K. E. The Heat Conduction Renaissance. 17th IEEE Intersociety Conference on Thermal and Thermomechanical Phenomena in Electronic Systems (ITherm); IEEE: 2018; pp 1396−1402.

(6) Suryavanshi, S. V.; Pop, E. S2DS: Physics-Based Compact Model for Circuit Simulation of Two-Dimensional Semiconductor Devices Including Non-Idealities. *J. Appl. Phys.* **2016**, *120*, 224503.

(7) Islam, S.; Li, Z.; Dorgan, V. E.; Bae, M. H.; Pop, E. Role of Joule Heating on Current Saturation and Transient Behavior of Graphene Transistors. *IEEE Electron Device Lett.* **2013**, *34* (2), 166−168.

(8) Yalon, E.; Mcclellan, C. J.; Smithe, K. K. H.; Xu, R. L.; Rojo, M. M.; Suryavanshi, S. V.; Gabourie, A. J.; Neumann, C. M.; Xiong, F.; Pop, E.; et al. Energy Dissipation in Monolayer MoS$_2$ Electronics. *Nano Lett.* **2017**, *17* (6), 3429−3433.

(9) Yalon, E.; Aslan, Ö. B.; Smithe, K. K. H.; McClellan, C. J.; Suryavanshi, S. V.; Xiong, F.; Sood, A.; Neumann, C. M.; Xu, X.; Goodson, K. E.; Heinz, T. F.; Pop, E. Temperature-Dependent Thermal Boundary Conductance of Monolayer MoS$_2$ by Raman

Thermometry. *ACS Appl. Mater. Interfaces* **2017**, *9* (49), 43013−43020.

(10) Yasaei, P.; Foss, C. J.; Karis, K.; Behranginia, A.; El-Ghandour, A. I.; Fathizadeh, A.; Olivares, J.; Majee, A. K.; Foster, C. D.; Khalili-Araghi, F.; Aksamija, Z.; Salehi-Khojin, A. Interfacial Thermal Transport in Monolayer $MoS_2$- and Graphene-Based Devices. *Adv. Mater. Interfaces* **2017**, *4*, 1700334.

(11) Liu, Y.; Ong, Z.; Wu, J.; Zhao, Y.; Watanabe, K.; Taniguchi, T.; Chi, D.; Zhang, G.; Thong, J. T. L.; Qiu, C.-W.; Hippalgaonkar, K. Thermal Conductance of the 2D $MoS_2$/h-BN and Graphene/h-BN Interfaces. *Sci. Rep.* **2017**, *7*, 43886.

(12) Yuan, P.; Li, C.; Xu, S.; Liu, J.; Wang, X. Interfacial Thermal Conductance between Few to Tens of Layered-$MoS_2$ and c-Si: Effect of $MoS_2$ Thickness. *Acta Mater.* **2017**, *122*, 152−165.

(13) Das, S.; Appenzeller, J. Screening and Interlayer Coupling in Multilayer $MoS_2$. *Phys. Status Solidi RRL* **2013**, *7* (4), 268−273.

(14) Cheng, R.; Jiang, S.; Chen, Y.; Liu, Y.; Weiss, N.; Cheng, H. C.; Wu, H.; Huang, Y.; Duan, X. Few-Layer Molybdenum Disulfide Transistors and Circuits for High-Speed Flexible Electronics. *Nat. Commun.* **2014**, *5*, 5143.

(15) Kim, J. Y.; Choi, S. M.; Seo, W. S.; Cho, W. S. Thermal and Electronic Properties of Exfoliated Metal Chalcogenides. *Bull. Korean Chem. Soc.* **2010**, *31* (11), 3225−3227.

(16) Lindroth, D. O.; Erhart, P. Thermal Transport in van Der Waals Solids from First-Principles Calculations. *Phys. Rev. B: Condens. Matter Mater. Phys.* **2016**, *94*, 115205.

(17) Jiang, P.; Qian, X.; Gu, X.; Yang, R. Probing Anisotropic Thermal Conductivity of Transition Metal Dichalcogenides $MX_2$ (M = Mo, W and X = S, Se) Using Time-Domain Thermoreflectance. *Adv. Mater.* **2017**, *29* (36), 1701068.

(18) Wei, Z.; Yang, J.; Chen, W.; Bi, K.; Li, D.; Chen, Y. Phonon Mean Free Path of Graphite along the c-Axis. *Appl. Phys. Lett.* **2014**, *104*, 081903.

(19) Fu, Q.; Yang, J.; Chen, Y.; Li, D.; Xu, D. Experimental Evidence of Very Long Intrinsic Phonon Mean Free Path along the c-Axis of Graphite. *Appl. Phys. Lett.* **2015**, *106*, 031905.

(20) Zhang, H.; Chen, X.; Jho, Y. D.; Minnich, A. J. Temperature-Dependent Mean Free Path Spectra of Thermal Phonons along the c-Axis of Graphite. *Nano Lett.* **2016**, *16* (3), 1643−1649.

(21) Esfarjani, K.; Chen, G.; Stokes, H. T. Heat Transport in Silicon from First-Principles Calculations. *Phys. Rev. B: Condens. Matter Mater. Phys.* **2011**, *84*, 085204.

(22) Sood, A.; Cho, J.; Hobart, K. D.; Feygelson, T. I.; Pate, B. B.; Asheghi, M.; Cahill, D. G.; Goodson, K. E. Anisotropic and Inhomogeneous Thermal Conduction in Suspended Thin-Film Polycrystalline Diamond. *J. Appl. Phys.* **2016**, *119*, 175103.

(23) Muratore, C.; Varshney, V.; Gengler, J. J.; Hu, J. J.; Bultman, J. E.; Smith, T. M.; Shamberger, P. J.; Qiu, B.; Ruan, X.; Roy, A. K.; Voevodin, A. A. Cross-Plane Thermal Properties of Transition Metal Dichalcogenides. *Appl. Phys. Lett.* **2013**, *102*, 081604.

(24) Sood, A.; Cheaito, R.; Bai, T.; Kwon, H.; Wang, Y.; Li, C.; Yates, L.; Bougher, T.; Graham, S.; Asheghi, M.; Goorsky, M.; Goodson, K. E. Direct Visualization of Thermal Conductivity Suppression Due to Enhanced Phonon Scattering near Individual Grain Boundaries. *Nano Lett.* **2018**, *18* (6), 3466−3472.

(25) Regner, K. T.; Sellan, D. P.; Su, Z.; Amon, C. H.; McGaughey, A. J. H.; Malen, J. A. Broadband Phonon Mean Free Path Contributions to Thermal Conductivity Measured Using Frequency Domain Thermoreflectance. *Nat. Commun.* **2013**, *4*, 1640.

(26) Shanks, H. R.; Maycock, P. D.; Sidles, P. H.; Danielson, G. C. Thermal Conductivity of Silicon from 300 to 1400 K. *Phys. Rev.* **1963**, *130* (5), 1743−1748.

(27) Buyco, E. H.; Davis, F. E. Specific Heat of Aluminum from Zero to Its Melting Temperature and Beyond. Equation for Representation of the Specific Heat of Solids. *J. Chem. Eng. Data* **1970**, *15* (4), 518−523.

(28) Flubacher, P.; Leadbetter, A. J.; Morrison, J. A. The Heat Capacity of Pure Silicon and Germanium and Properties of Their Vibrational Frequency Spectra. *Philos. Mag.* **1959**, *4* (39), 273−294.

(29) Minnich, A. J. Thermal Phonon Boundary Scattering in Anisotropic Thin Films. *Appl. Phys. Lett.* **2015**, *107*, 183106.

(30) Gu, X.; Li, B.; Yang, R. Layer Thickness-Dependent Phonon Properties and Thermal Conductivity of $MoS_2$. *J. Appl. Phys.* **2016**, *119*, 085106.

(31) Meyer, K. E.; Cheaito, R.; Paisley, E.; Shelton, C. T.; Braun, J. L.; Maria, J.; Ihlefeld, J. F.; Hopkins, P. E. Crystalline Coherence Length Effects on the Thermal Conductivity of MgO Thin Films. *J. Mater. Sci.* **2016**, *51* (23), 10408−10417.

(32) Jang, H.; Wood, J. D.; Ryder, C. R.; Hersam, M. C.; Cahill, D. G. Anisotropic Thermal Conductivity of Exfoliated Black Phosphorus. *Adv. Mater.* **2015**, *27* (48), 8017−8022.

(33) Yuan, P.; Wang, R.; Wang, T.; Wang, X.; Xie, Y. Nonmonotonic Thickness-Dependence of In-Plane Thermal Conductivity of Few-Layered $MoS_2$: 2.4 to 37.8 nm. *Phys. Chem. Chem. Phys.* **2018**, *20* (40), 25752−25761.

(34) Muratore, C. University of Dayton, Dayton, OH. Personal Communication, 2017.

(35) Koh, Y. K.; Cahill, D. G. Frequency Dependence of the Thermal Conductivity of Semiconductor Alloys. *Phys. Rev. B: Condens. Matter Mater. Phys.* **2007**, *76*, 075207.

(36) Wilson, R. B.; Feser, J. P.; Hohensee, G. T.; Cahill, D. G. Two-Channel Model for Nonequilibrium Thermal Transport in Pump-Probe Experiments. *Phys. Rev. B: Condens. Matter Mater. Phys.* **2013**, *88*, 144305.

(37) Wilson, R. B.; Cahill, D. G. Anisotropic Failure of Fourier Theory in Time-Domain Thermoreflectance Experiments. *Nat. Commun.* **2014**, *5*, 5075.

(38) Koh, Y. K.; Cahill, D. G.; Sun, B. Nonlocal Theory for Heat Transport at High Frequencies. *Phys. Rev. B: Condens. Matter Mater. Phys.* **2014**, *90*, 205412.

(39) Regner, K. T.; Wei, L. C.; Malen, J. A. Interpretation of Thermoreflectance Measurements with a Two-Temperature Model Including Non-Surface Heat Deposition. *J. Appl. Phys.* **2015**, *118*, 235101.

(40) Yang, F.; Dames, C. Heating-Frequency-Dependent Thermal Conductivity: An Analytical Solution from Diffusive to Ballistic Regime and its Relevance to Phonon Scattering Measurements. *Phys. Rev. B: Condens. Matter Mater. Phys.* **2015**, *91*, 165311.

(41) Sun, B.; Gu, X.; Zeng, Q.; Huang, X.; Yan, Y.; Liu, Z.; Yang, R.; Koh, Y. K. Temperature Dependence of Anisotropic Thermal-Conductivity Tensor of Bulk Black Phosphorus. *Adv. Mater.* **2017**, *29*, 1603297.

(42) Chen, S.; Sood, A.; Pop, E.; Goodson, K. E.; Donadio, D. Strongly Tunable Anisotropic Thermal Transport in $MoS_2$ by Strain and Lithium Intercalation: First Principles Calculations. *2D Mater.* **2019**. In press. DOI: 10.1088/2053-1583/ab0715.

(43) Wakabayashi, N.; Smith, H. G.; Nicklow, R. M. Lattice Dynamics of Hexagonal $MoS_2$ Studied by Neutron Scattering. *Phys. Rev. B* **1975**, *12* (2), 659−663.

(44) Zhu, G.; Liu, J.; Zheng, Q.; Zhang, R.; Li, D.; Banerjee, D.; Cahill, D. G. Tuning Thermal Conductivity in Molybdenum Disulfide by Electrochemical Intercalation. *Nat. Commun.* **2016**, *7*, 13211.

(45) Sood, A.; Xiong, F.; Chen, S.; Wang, H.; Selli, D.; Zhang, J.; McClellan, C. J.; Sun, J.; Donadio, D.; Cui, Y.; Pop, E.; Goodson, K. E. An Electrochemical Thermal Transistor. *Nat. Commun.* **2018**, *9*, 4510.

(46) Koh, Y. K.; Bae, M. H.; Cahill, D. G.; Pop, E. Heat Conduction across Monolayer and Few-Layer Graphenes. *Nano Lett.* **2010**, *10* (11), 4363−4368.

(47) Mleczko, M. J.; Xu, R. L.; Okabe, K.; Kuo, H.-H.; Fisher, I. R.; Wong, H.-S. P.; Nishi, Y.; Pop, E. High Current Density and Low Thermal Conductivity of Atomically Thin Semimetallic $WTe_2$. *ACS Nano* **2016**, *10* (8), 7507−7514.

(48) Kong, S.; Wu, T.; Yuan, M.; Huang, Z.; Meng, Q.-L.; Jiang, Q.; Zhuang, W.; Jiang, P.; Bao, X. Dramatically Enhanced Thermoelectric Performance of $MoS_2$ by Introducing $MoO_2$ Nanoinclusions. *J. Mater. Chem. A* **2017**, *5*, 2004−2011.

(49) Giannozzi, P.; Baroni, S.; Bonini, N.; Calandra, M.; Car, R.; Cavazzoni, C.; Ceresoli, D.; Chiarotti, G. L.; Cococcioni, M.; Dabo, I.; Dal Corso, A.; de Gironcoli, S.; Fabris, S.; Fratesi, G.; Gebauer, R.; Gerstmann, U.; Gougoussis, C.; Kokalj, A.; Lazzeri, M.; Martin-Samos, L.; Marzari, N.; Mauri, F.; Mazzarello, R.; Paolini, S.; Pasquarello, A.; Paulatto, L.; Sbraccia, C.; Scandolo, S.; Sclauzero, G.; Seitsonen, A. P.; Smogunov, A.; Umari, P.; Wentzcovitch, R. M. QUANTUM ESPRESSO: A Modular and Open-Source Software Project for Quantum Simulations of Materials. *J. Phys.: Condens. Matter* **2009**, *21* (39), 395502.

(50) Perdew, J. P.; Zunger, A. Self-Interaction Correction to Density-Functional Approximations for Many-Electron Systems. *Phys. Rev. B: Condens. Matter Mater. Phys.* **1981**, *23* (10), 5048−5079.

(51) Hartwigsen, C.; Goedecker, S.; Hutter, J. Relativistic Separable Dual-Space Gaussian Pseudopotentials from H to Rn. *Phys. Rev. B: Condens. Matter Mater. Phys.* **1998**, *58* (7), 3641−3662.

(52) Monkhorst, H. J.; Pack, J. D. Special Points for Brillouin-Zone Integrations. *Phys. Rev. B* **1976**, *13* (12), 5188−5192.

(53) Baroni, S.; De Gironcoli, S.; Dal Corso, A.; Giannozzi, P. Phonons and Related Crystal Properties from Density-Functional Perturbation Theory. *Rev. Mod. Phys.* **2001**, *73* (2), 515−562.

(54) Li, W.; Carrete, J.; Katcho, N. A.; Mingo, N. ShengBTE: A Solver of the Boltzmann Transport Equation for Phonons. *Comput. Phys. Commun.* **2014**, *185* (6), 1747−1758.